Controlled Size Reduction of Liquid Exfoliated Graphene Micro-Sheets via Tip Sonication

crystals

MDPI

Article

Controlled size reduction of liquid exfoliated graphene micro sheets v*ia* tip sonication

Chiara Di Berardino[1], Péter Bélteky[2], Fabian Schmitz[1,3], Francesco Lamberti[4], Enzo Menna[4], Ákos Kukovecz[2] and Teresa Gatti[1,3*]

[1] Institute of Physical Chemistry, Justus Liebig University, Heinrich Buff Ring 17, 35392 Giessen, Germany; chiara.diberardino@chemie.uni-giessen.de, fabian.schmitz@phys.chemie.uni-giessen.de

[2] University of Szeged, Interdisciplinary Excellence Centre, Department of Applied and Environmental Chemistry, H-6720, Rerrich Béla tér 1, Szeged, Hungary; peti0225@gmail.com, kakos@chem.u-szeged.hu

[3] Center for Materials Research (LaMa), Justus Liebig University, Heinrich Buff Ring 16, 35392 Giessen, Germany

[4] Department of Chemical Sciences, University of Padova, via Marzolo 1, 35131 Padova, Italy; francesco.lamberti@unipd.it, enzo.menna@unipd.it

* Correspondence: teresa.gatti@phys.chemie.uni-giessen.de

Received: date; Accepted: date; Published: date

Abstract: Liquid exfoliation of three-dimensional bulk solids having an inherent layered structure is an effective and scalable method to produce stable to re-aggregation colloidal inks of 2D materials suitable for solution processing. Shear-mixing is a relatively gentle technique that allows the exfoliation by preserving the native lateral size of the 3D precursors, while tip sonication often leads to extensive structural damage, producing 2D sheets where many edge defects are introduced. We present here a mixed approach to obtain liquid dispersions of few-layers graphene flakes where the average lateral size of the colloids can be tuned in a controlled way. The strategy relies on the application of defined tip sonication steps on graphene inks prepared previously through the use of a shear mixer, in this way starting from already exfoliated micro-sheets with limited amount of edge defects. Our approach could represent a valuable method to prepare 2D materials inks with variable size distribution, as differences in this parameter could have a significant impact on the electronic behavior of the final material and thus on its field of application.

Keywords: few-layers graphene; liquid phase exfoliation; graphene ink; tip sonication; graphene sheets

1. Introduction

The production of 2D materials through scalable methods that can preserve their quality and ensure their industrial exploitation in a wide variety of devices[1–4] and applications[5–8] is a major concern in nowadays applied research.[9] Bottom-up approaches to produce them, such as epitaxial growth on catalytic substrates through chemical vapor deposition[10] or organic synthesis starting from precursor molecules,[11] are not advantageous from an economical point of view for industrial-scale production, unless highly pure single layer species are required. In order to find a cheaper and less hazardous process for large scale graphene production, the liquid-phase exfoliation (LPE) methods have been developed in the last few years.[12,13] These techniques provide the system with the required energy to overcome the van der Waals forces between layers in 3D crystals without increasing the in-plane defects degree. The LPE process generally involves threes steps, namely the dispersion of the bulk material in a given solvent or water/surfactant solution, the exfoliation itself and the purification. The last step (normally carried out through liquid cascade centrifugation) is necessary for the separation of the exfoliated fraction from the un-exfoliated one and it affects the final concentration

of the 2D material ink. The choice of the solvent is also crucial as it determines the strength of the solute-solvent interactions. The ideal solvent should minimize the interfacial tension between the liquid and the 2D flakes in order to avoid the flakes to re-adhere to each other. In the case of LPE of graphene, the best solvent identified to fulfill these requirements is undoubtedly N-cyclohexyl-2-pyrrolidone (CHP), given the match in surface tension with that of graphite ($\gamma \sim 40$ mJ m^{-2}).[14]

Among LPE methods it is convenient to distinguish between the use of shear-mixer type devices and tip sonicators. The former feature an instrument head made of a rotor and stator: the rotation of the inner part causes the formation of strong shear and thrust forces at which the mixture is subjected. The procedure is controlled by hydrodynamic shear-forces under laminar flow in complete absence of turbulence, avoiding the formation of in-plane defects. Paton et al. have shown that exfoliation occurs whenever the local shear rate exceeds a critical value of around 10^4 s^{-1}.[14] On the other hand, tip sonication consists in a ultrasound-assisted exfoliation, during which hydrodynamic, shear-forces associated with cavitation act on the bulk material and induce exfoliation. The exfoliation mechanism is accompanied by fracturing processes, due to shockwaves generated by immediately adjacent inertial cavitation activity, with the resulting effect of producing sheets with an elevated number of edge defects.[15]

Here we report on the use of a two steps LPE method that allows the control of the average size of few layer graphene sheets dispersed in CHP, with significant relevance for the future production of size-defined graphene inks to be used for solution processing. This method consists in the previous production of graphene micro sheets through shear-mixing starting from large-size graphite crystals followed by the tunable reduction of the lateral sizes applying tip sonication protocols. We provide a complete physico-chemical characterization of the thus produced size-controlled graphene inks that allows the rationalization of the the effects of the sonication parameters employed on such a post-synthetic method.

2. Materials and Methods

The EXG 3000 ink in CHP was prepared according to the procedure reported previously in ref [16]. Solvents were from Sigma-Aldrich and used as received. Shear-mixing LPE was carried out with an IKA T25 digital shear mixer operating at 8000 rpm. The sample was cooled to 0 °C with an ice bath during operation. Tip sonication was carried on a Baudelin Sonopuls tip sonicator operating at a 40% and 60% power using pulses of 3s on/ 3s off. The samples were contained in 250 ml quartz beckers kept in an ice bath. Raman spectroscopy was carried out using a Senterra Raman microscope working with an excitation laser at $\lambda = 532$ nm. All the samples were prepared by two consecutive centrifugation steps of a mixture made with some drops of graphene suspension in EtOH to get rid of the non-volatile solvent. The graphene/EtOH suspension was deposited on pre-cleaned oxidized Si wafer and the solvent was evaporated. The focus was obtained with a 50x lens. The instrumental settings were optimized and used for all the measurements: 5 sec, 40 co-additions, 5 mW of laser power. DLS measurements were conducted with Malvern Zetasizer Nano-ZS device. The DLS system was operated by the software Zetasizer from Malvern Panlytical. Instrumental settings adopted were the following: 20 °C, toluene as solvent with a refractive index of 1.496 and graphene refractive index 2.411. The samples were prepared dissolving a drop of graphene mixture in toluene. The samples were measured in Rotilabo® precision glass cuvettes with a light path of 10 mm and a volume of 3.5 mL. TEM images were acquired on a FEI Tecnai G2 microscope operating at 100 kV. HR-TEM and SAED patterns were captured from samples created by drop casting lacy carbon grids with a FEI Tecnai G2 20 X Twin instrument using 200 kV accelerating voltage. TGA was run in air on ~1 mg sample using a Q5000 IR model TA instrument with the method of starting at 100 °C and kept isothermal for 20 min, then ramping to 10 °C min^{-1} up to 1000 °C. UV-Visible absorption spectra were acquired on a Goebel Uvikon spectrophotometer on original suspension in CHP further diluted with dimethylformamide to achieve optical densities around 0.5.

3. Results and Discussion

Some of us reported in a previous work[16] the production of LPE graphene micro sheets of lateral sizes up to 50 μm or more and average number of layers around 5 starting from high-quality Madagascar graphite, employing the shear mixing method introduced by Paton et al. in CHP.[14] The resulting ink is a stable to re-aggregation colloidal suspension, characterized by a concentration of graphene sheets in the range of 250-300 μg ml^{-1}.[16] This colloidal sample is named EXG 3000 after the purification protocol employed. This consists in three subsequent centrifugation steps at increasing centrifugation speed, the last one being indeed carried out at 3000 rpm (1170×g) and allowing the isolation of the most exfoliated fraction within the mixture that underwent LPE. To this graphene micro sheets ink, tip sonication processes of different duration and power have been applied and the resulting products have been characterized by Raman spectroscopy, dynamic light scattering (DLS), transmission electron microscopy (TEM) and thermogravimetric analysis (TGA) to provide a detailed picture in terms of average flakes sizes and defects distribution.

More in detail, three different ultrasonication treatments were applied starting from EXG 3000, which are summarized in Table 1 in terms of sonication power and time.

Table 1. Conditions applied for the ultrasonication of the graphene ink EXG 3000.

Sample name	Starting graphitic suspension	Nominal electrical input power (%)	Sonication time (min)
EXG 3000 40 min	EXG 3000	40 %	2 × 20 [1]
EXG 3000 100 min	EXG 3000 40 min	40 %	2 × 30 [1]
EXG 3000 120 min	EXG 3000	60 %	2 × 60 [1]

[1] Between the two intervals a pause of 5 min was applied

As it can be inferred from this table, the protocol employed aims at verifying whether two subsequent sonication steps at short times and medium power (the first two entries in the table) differs from the application of one single long step at high power (last entry). The first-time interval of the two-step case was kept lower than 1 h to verify the effect of a relatively short initial sonication.

The products were first analyzed via Raman spectroscopy (Figure 1). In Figure 1a a section of the Raman spectra of the different samples is reported and, precisely, in the range in which the D (defects-related) and G (sp^2 structure-related) bands are located. The small shoulder appearing on the high wavenumber side of the G band is the so-called D′ band.[17,18] The intensity ratio between the D band (I_D) over the G band (I_G) was evaluated for the three samples and for EXG 3000 and the resulting values are summarized in Table 2.

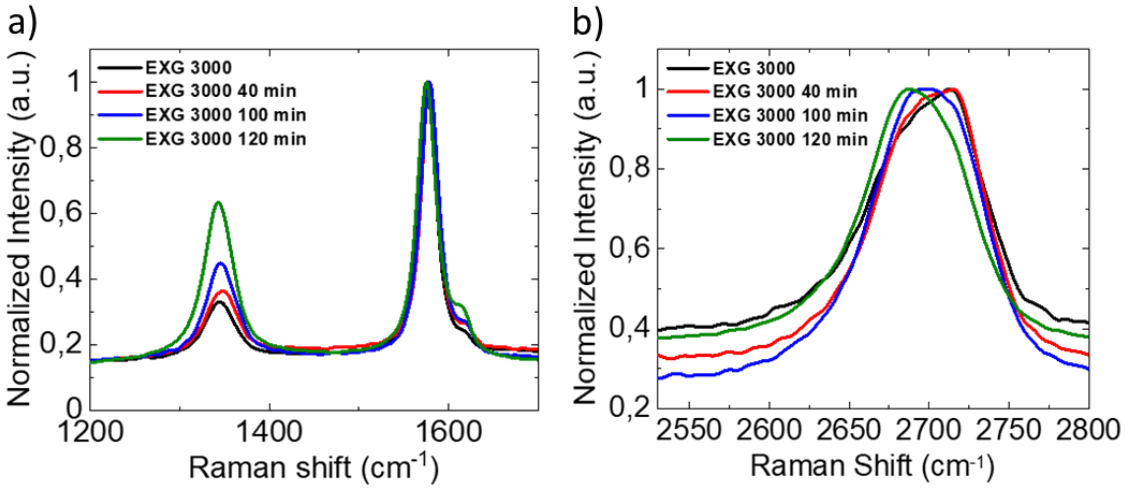

Figure 1. Raman spectroscopy analysis on the ultrasonicated EXG 3000 samples and on pristine EXG 3000. a) Detail of the D and G bands with relative intensity normalized on the G peak. b) Detail of the 2D band.

Table 2. Relevant intensity ratios between Raman peaks in Figure 1a.

Sample name	Average I_D/I_G[1]	Average $I_D/I_{D'}$[1]
EXG 3000	0.382 ± 0.030	1.15 ± 0.02
EXG 3000 40 min	0.390 ± 0.025	0.97 ± 0.02
EXG 3000 100 min	0.431 ± 0.021	1.75 ± 0.01
EXG 3000 120 min	0.667 ± 0.058	1.47 ± 0.04

[1] Average of five measurements in different points of the sample

The D band intensity clearly increases with the time and power of sonication applied. This is particularly evident for the sample sonicated in one single step for a long time and with a high power (EXG 3000 120 min), while for the sample sonicated at the shorter time slot (EXG 3000 40 min) the increase is relatively low. The observed trend could be related to the presence of a greater number of defects either at the edges or in the basal plane. In the first case, a greater number of edges could be correlated to a decrease of graphene flakes lateral size, while in the second case defects located in the basal plane could be generated as a side-effect of the sonication energy applied. To distinguish between the two types of defects, the intensity of the D band (I_D) over the D′ band ($I_{D'}$) was evaluated in order to verify the nature of defects (Table 2), according to Eckmann et al., that demonstrated how the value of the $I_D/I_{D'}$ ratio depends only on the types of defects rather than on their quantity.[18] For each sample, the value of the $I_D/I_{D'}$ ratio evaluated is smaller than 3.5, a threshold that indicates the presence of edge defects. The other kind of defects on the crystal structure of graphene, i.e. sp^3 carbons and vacancy, are characterized by higher ratio values. Hence, the major effect of the sonication step was to reduce the graphene flakes size. The higher the sonication power, the smaller the flakes and consequently the more the edges.

The analysis of the 2D band (Figure 1b) shed light on other interesting information about the degree of exfoliation and how it is affected by the sonication step. Indeed, 2D band shape and shift of the maximum are heavily affected by the number of graphene layers present in an analysed sample.[17] In single layer graphene, the intensity of the 2D (I_{2D}) peak should be roughly four times I_G and it should quickly decrease as the number of layers increases. In the here analysed samples, I_{2D} was found to be about half of I_G. Hence, in the inks few layers graphene predominates over single

layer. This result is also confirmed by the value of the full width at half maximum (FWHM) of the 2D band. The FWHM is larger than 50 cm^{-1} and it almost doubles the one of the single layer graphene 2D peak. Nonetheless, the corresponding peaks show a progressive down-shift of more than 25 cm^{-1} in respect to the starting material (Figure1b), accountable to a contemporary flake exfoliation during the sonication step.[19] Through the qualitative analysis of the 2D band shape, within which two components can be distinguished at around 2725 and 2675 cm-1 that change in relative intensity in relation to the number of layers in the specimen, as described in detail by Ferrari et al. in ref. [17], it is clear that the layers number progressively decreases by increasing time and power of sonication, as the intensity of the 2725 cm^{-1} component progressively decreases while the 2675 cm^{-1} one increases. Moreover, the more sonicated samples show a similar 2D band shape and so it is their degree of exfoliation. In particular, the sample to which one single long and high-power sonication step was applied (EXG 3000 120 min′) results to be the one in which the 2D band shape and position of the maximum recalls more closely that of single layer graphene. Indeed, the rate of exfoliation of graphene flakes becomes slower if their size decreases and as a consequence it is hard to further exfoliate the smaller flakes in suspension.[20]

The quantitative analysis of the flakes sizes was conducted via DLS. The technique could give reliable results on colloidal sizes only for spherical particles, while graphene flakes are almost completely planar. However, in this case DLS results were not used to define the hydrodynamic diameter of the flakes but to search for a trend resulting from the controlled sonication processes. Indeed, it is evident that smaller flakes can be obtained with longer and stronger ultrasonication step (Figure 2). In particular, DLS analysis reveals that flakes size drastically decreases after 40 min of sonication but there are just minor changes for further sonication times. In fact, the hydrodynamic diameter obtained for the sample after the 120 min cycle sonication is similar to the one obtained after the 100 min cycle in two consecutive steps of 40 and 60 min.

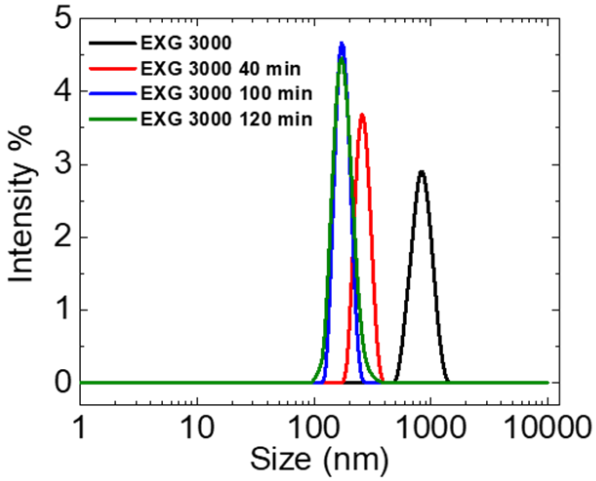

Figure 2. DLS spectra of the ultrasonicated EXG 3000 samples and of pristine EXG 3000.

More detailed information on the sample morphologies are obtained by performing TEM and high-resolution (HR-TEM) analysis. Figure 3 reports the TEM images at lower and higher resolution of the starting LPE ink EXG 3000. The considerable lateral extension of the graphene sheets contained within the colloidal suspension is well evident from the left image, where the flakes appear to be covering a large part of the TEM grid. More in detail, from the right image it is possible to notice that such a remarkable size extension (which originates by the fact that shear mixing is not a destructive method to perform graphite exfoliation and the starting Madagascar graphite sample was constituted of very big crystals[16]) causes the flakes to fold in some point, forming sort of wrinkles. Selected area electron diffraction (SAED) in Figure 3c shows the presence of reflections typical of a graphite-like sp2 carbon phase (those indicated as 100, 110 and 112) and a very weak signal of a reflection assignable to a diamond-like phase, and thus sp3 carbon (the one indicated as 311), probably due to the existing sp3 defects in the sample that give rise to a non-zero D-band in Figure 1a (black line).12

Given the lateral extension of the sample it is difficult to identify edges and therefore such a weak sp3 carbon signal could be due to defects present in the basal plane of the flakes (which could have been present already in the pristine graphite).

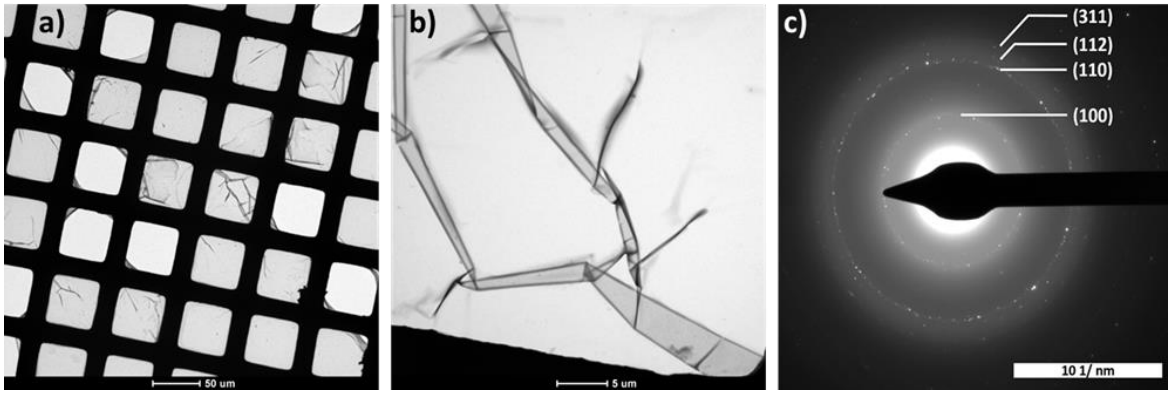

Figure 3. TEM images of EXG 3000 showing the considerable size of the graphene flakes present in the sample (left image at lower magnification) and their wrinkled nature (right image at higher magnification).

The sonication at 40 min of EXG 3000 at medium power (EXG 3000 40 min) causes a considerable reduction of the flake sizes that do not surpass the 1 μm threshold, with the smallest components also featuring lateral extensions of 50-100 nm (Figure 4a). HR-TEM allows to examine precisely the nature of the exfoliation, confirming what seen from Raman analysis of the 2D peak, i.e. a not considerable difference in number of stacked layers from the pristine EXG 3000 sample (around 5, Figure 4b).

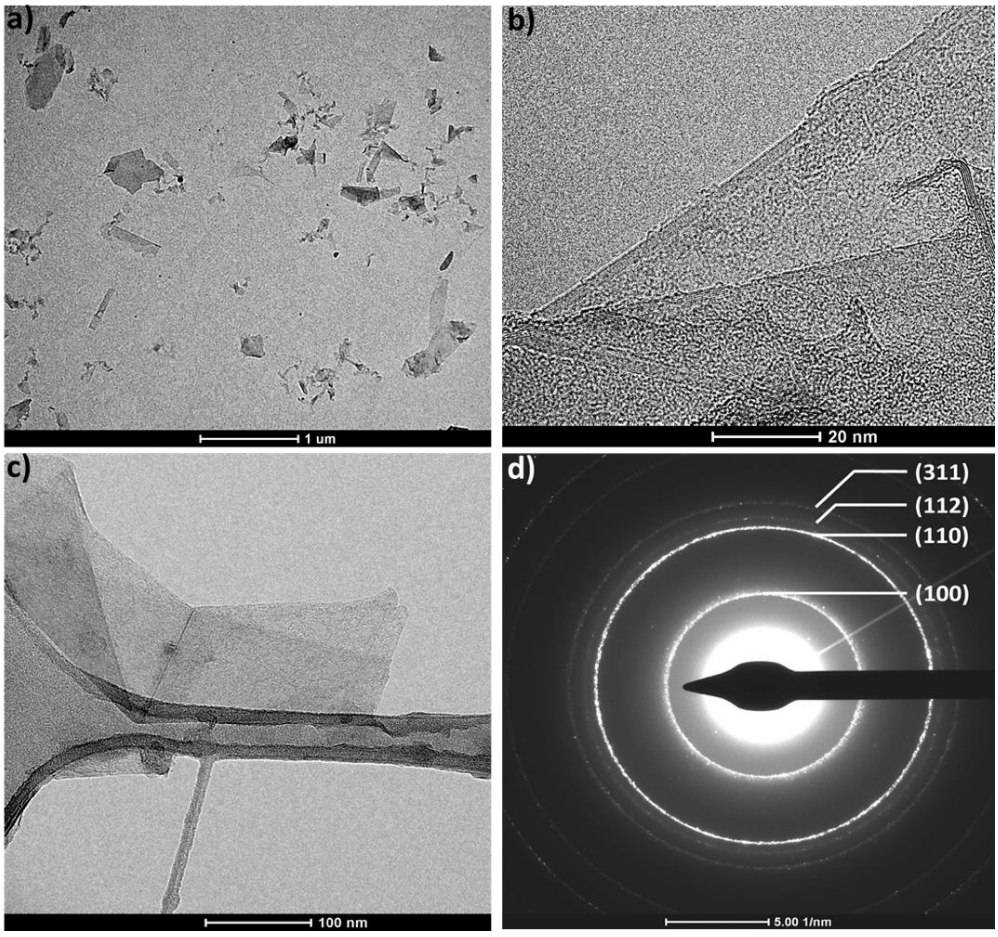

Figure 4. Transmission electron microscopy characterization of the EXG 3000 40 min sample. a) Low magnification TEM image of the sample. b) HR-TEM high magnification detail showing a number of superimposed graphene layers in the samples equal to 5. c) HR-TEM detail on the geometrical shape of the flake edges. d) SAED of the edges with indicated number of the identified reflections (see text for speciation).

While the breaking of the flakes is extensive, the action of the sonication process on the 2D material edges appears to be relatively regular, with the overall morphology in these parts maintaining defined angles and straight lines, and with no sign of holes formation within the basal planes. The nature of the defects at the edges is difficult to predict, nonetheless selected area electron diffraction (SAED) could provide interesting hints on this aspect if addressed specifically onto this part of the flakes. Figure 4s shows the SAED patter obtained by selectively focusing on a flake edge, from which the graphite-like reflections 100, 110 and 112 are still detected and the diamond-like reflection 311 results considerably more visible than in the starting EXG 300 sample (Figure 3d).[21] This increase in intensity could be an indication that some of the defects created at the sheet edges through prolonged sonication are carbon atoms in tetrahedral form. On the other hand, their distribution should give rise to areas with a crystalline order (also if very small ones), as otherwise they could not give rise to a detectable diffraction pattern.

The average size of the flakes that underwent the second step of sonication at low power (EXG 3000 100 min) and that of those coming from the single step high power treatment (EXG 3000 120 min) resulted to be very similar and extending in the range of few hundreds nm (between 100 and 500 nm maximum). The latter sample was further analyzed through HR-TEM, showing the formation of peculiar morphologies at the edges, where irregular shapes are found as a result of the aggressive treatment. Figure 5 reports a summary of these features: in the two top panels (Figure 5a and 5b) it is possible to notice the formation of holes in the basal plane of the flakes having different dimensionalities and an irregular geometry. These patterns are anyway to be considered as edges and not as in plane defects, given their considerable extension. The increased level of exfoliation is seen by focusing on edge areas where the highly irregular trend is not present, as the one highlighted in Figure 5c. Number of superimposed graphene flakes between 2 and 3 are thus identified, while monolayers are mainly found where the disordered damage is located, with an example in Figure 5d. In these rugged edges the same sp^3 carbon SAED signature described above (Figure 4d) can be detected, together with those typical of graphite (inset of Figure 5d).

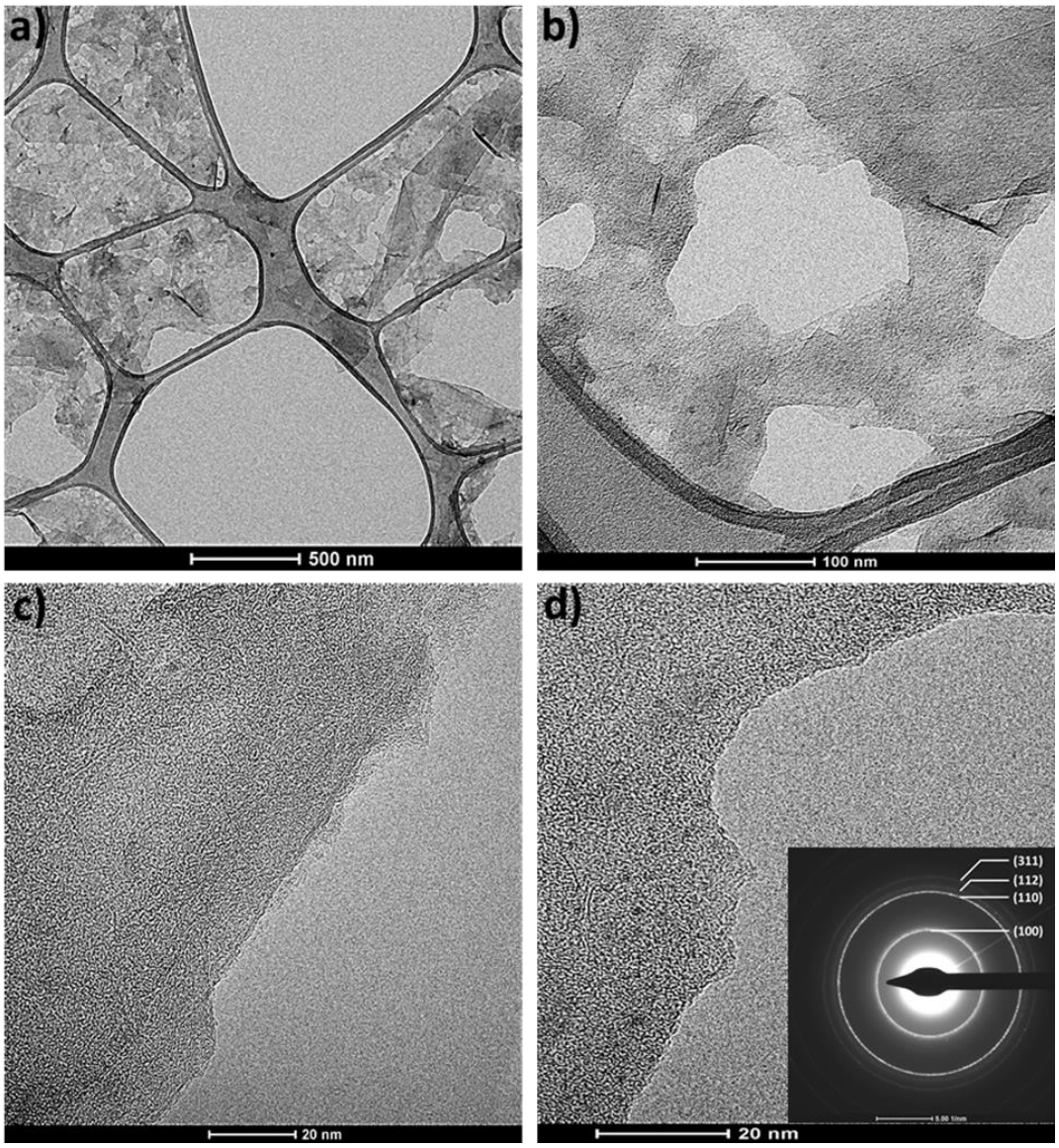

Figure 5. HR-TEM images of EXG 3000 120 min. The pronounced nature of the damage caused by prolonged sonication of the starting EXG 3000 sample is seen in these images with a), b) the generation of holes in the basal planes of the nano-sheets, c) a more extensive exfoliation and d) a rugged morphology at the edges.

The sonicated samples were further analyzed for their thermal behavior, by performing TGA in air to determine the decomposition temperature. Already for EXG 3000 a not net transition was identified (like the one of pure graphite), as the material was found to start with a little degradation already at around 250 °C. Nonetheless a decomposition temperature of 490 ° C was extrapolated at the intersection of two linear fits encountering where the slope of the decomposition curve was most pronounced.[16] The sonication treatment increases considerably this progressive weight loss as a result of increased temperature in the presence of oxygen, with an almost 80% of the initial mass of the specimen decomposed at 450°C and the remaining 20% completed within a 50 °C step ahead for the EXG 3000 sample sonicated for 40 min (red curve in Figure 6). The second step of sonication then further worsen the thermal stability (blue curve in Figure 6), with an initial drop of weight even more considerable. On the other hand, the sample sonicated in one single high power and long step features a thermal behavior similar to the EXG 3000 40 min one, indicating that the two materials could have similar stabilities, despite the different morphology and average sizes.

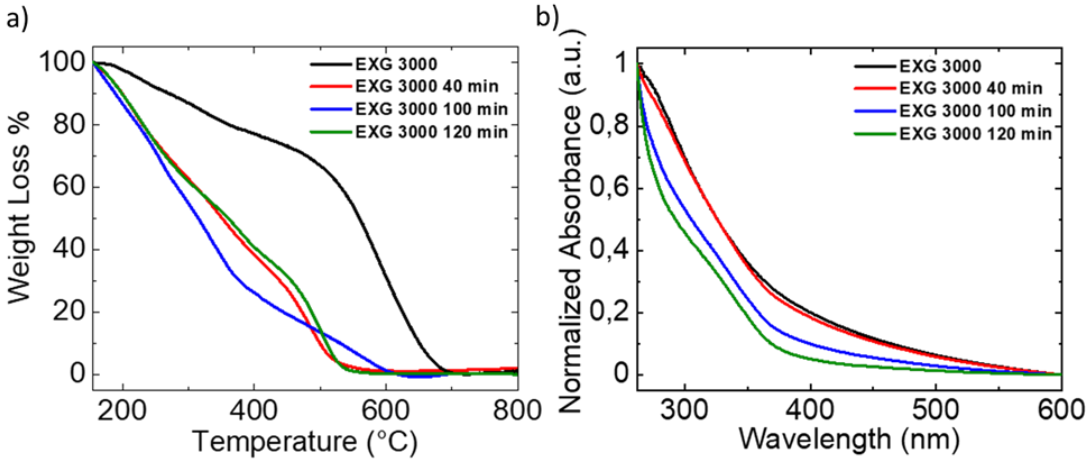

Figure 6. a) Thermograms in air of the ultrasonicated EXG 3000 samples and of pristine EXG 3000. b) UV-Visible absorption spectra of the ultrasonicated EXG 3000 samples and of pristine EXG 3000.

We finally carried out an UV-Visible spectroscopic characterization of the ultrasonicated samples and compared their spectra with that of pristine EXG 3000, in order to verify the effect of extensive flakes damage on the optical and plasmonic properties of the dispersed graphene sheets. As it can be inferred from Figure 6b, a constant decrease in absorption along the whole visible range is detected for the two samples that underwent the longest sonication treatments (i.e. EXG 3000 100 and 120 min), while the sample sonicated for the shortest time (EXG 3000 40 min) maintains an absorption profile similar to that of the pristine material. Such a deterioration in the optical response resulting for the smallest produced nanosheets points out at a modification of the plasmonic response in the material, where likely electrons have lower freedom to move along a surface with a high amount of defects compared to the case of an extended micro sheet and thus start to feel a sort of confinement (which at the extreme cases would lead to the obtainment of graphene quantum dots, thus fully 0D materials).

4. Conclusions

We have reported here on a new approach to produce LPE graphene inks in CHP where the size and defects profiles of the suspended micro-sheets can be controlled by applying ultrasonication post-synthetic parameters. The size reduction of the starting micro-sheets was found to be considerable already at the shortest sonication time evaluated (40 min) leading to the formation of nano-sheets, suggesting that a very short or intermediate duration could provide lateral extensions that remain in the μm range. The effect of high power and time was seen to generate holes in the basal planes having variable sizes and geometries but still to be considered as edge defects given the relatively large extension, as the presence of real in plane defects should provide a different value for the $I_D/I_{D'}$ ration in the Raman spectra (these last type of defects are most likely individual sp^3 carbon moieties generated in a scattered manner on the sheets as an effect of, for example, a chemical treatment like functionalization[18]). In addition, an interesting perspective on the nature of the thus formed edge defects was provided through the use of SAED analysis, suggesting that ordered sp3 carbon structures could be formed at these sites as an effect of sonication.

Our data provide a valid platform for future studies aiming at determine the effect of different sizes and defects distribution on the properties of LPE graphene samples, with potential application also at other 2D materials inks. As a perspective for future work, a more thorough determination of the effect of shorter and less aggressive sonication procedures will be investigated, allowing to complete the scenario here presented, also through a better morphological characterization of the obtained species (for example through atomic force microscopy). In addition, a better understanding

of the modification induced in the electronic properties of the samples following the tip-sonication treatment is necessary. The changes observed in the optical absorption profiles of the sonicated materials compared to the pristine EXG 3000 sample provide first hints on existing variations in the plasmonic (and consequently electronic) response,[22] but other means have to be identified to better describe them, such as electrochemistry, conductive atomic force microscopy or charge transport measurements. The thus produced and characterized graphene inks could have a large interest for multiple applications where the size of the flakes and their defects identity is relevant, going from solution processed thin layers and devices to composites. They could even represent starting materials for selective chemical functionalization strategies[23-25] aiming at specific sites on the sheets[26,27] such as the edges or the holes in the basal plane formed after the most aggressive treatment described.

Funding: F.S. and T.G. thank the DFG for financial support via the Research Training Group 2204 "Substitute Materials for Sustainable Energy Technologies". T.G. further acknowledges the "Fonds der Chemischen Industrie" of the VCI. Funding from the Hungarian National Research Development and Innovation office through the project 2017-2.3.7-TÉT-IN-2017-00008 is also acknowledged by the contribution of Á. K.

Conflicts of Interest: The authors declare no conflict of interest.

References

1. Avouris, P. Graphene: Electronic and Photonic Properties and Devices. *Nano Lett.* 2010, *10*, 4285–4294. https://doi.org/10.1021/nl102824h.
2. Pumera, M. Graphene-Based Nanomaterials for Energy Storage. *Energy Environ. Sci.* 2011, *4*, 668–674. https://doi.org/10.1039/C0EE00295J.
3. Sahoo, N. G.; Pan, Y.; Li, L.; Chan, S. H. Graphene-Based Materials for Energy Conversion. *Adv. Mater.* 2012, *24*, 4203–4210. https://doi.org/10.1002/adma.201104971.
4. Cheng, J.; Wang, C.; Zou, X.; Liao, L. Recent Advances in Optoelectronic Devices Based on 2D Materials and Their Heterostructures. *Adv. Opt. Mater.* 2019, *7*, 1800441. https://doi.org/10.1002/adom.201800441.
5. Mosconi, D.; Blanco, M.; Gatti, T.; Calvillo, L.; Otyepka, M.; Bakandritsos, A.; Menna, E.; Agnoli, S.; Granozzi, G. Arene C–H Insertion Catalyzed by Ferrocene Covalently Heterogenized on Graphene Acid. *Carbon* 2019, *143*, 318-328. https://doi.org/10.1016/j.carbon.2018.11.010.
6. Gatti, T.; Manfredi, N.; Boldrini, C.; Lamberti, F.; Abbotto, A.; Menna, E. A D-π-A Organic Dye – Reduced Graphene Oxide Covalent Dyad as a New Concept Photosensitizer for Light Harvesting Applications. *Carbon* 2017, *115*, 746–753. https://doi.org/https://doi.org/10.1016/j.carbon.2017.01.081.
7. Yang, Y.; Asiri, A. M.; Tang, Z.; Du, D.; Lin, Y. Graphene Based Materials for Biomedical Applications. *Mater. Today* 2013, *16* (10), 365–373. https://doi.org/https://doi.org/10.1016/j.mattod.2013.09.004.
8. Cai, X.; Luo, Y.; Liu, B.; Cheng, H.-M. Preparation of 2D Material Dispersions and Their Applications. *Chem. Soc. Rev.* 2018, *47* (16), 6224–6266. https://doi.org/10.1039/C8CS00254A.
9. Milana, S. The Lab-to-Fab Journey of 2D Materials. *Nat. Nanotechnol.* 2019, *14* (10), 919–921. https://doi.org/10.1038/s41565-019-0554-3.
10. Novoselov, K. S.; Mishchenko, A.; Carvalho, A.; Castro Neto, A. H. 2D Materials and van Der Waals Heterostructures. *Science (80-.).* 2016, *353* (6298), aac9439. https://doi.org/10.1126/science.aac9439.
11. Yoon, K.-Y.; Dong, G. Liquid-Phase Bottom-up Synthesis of Graphene Nanoribbons. *Mater. Chem. Front.* 2020, *4* (1), 29–45. https://doi.org/10.1039/C9QM00519F.
12. Tao, H.; Zhang, Y.; Gao, Y.; Sun, Z.; Yan, C.; Texter, J. Scalable Exfoliation and Dispersion of Two-Dimensional Materials – an Update. *Phys. Chem. Chem. Phys.* 2017, *19* (2), 921–960. https://doi.org/10.1039/C6CP06813H.
13. Hu, G.; Kang, J.; Ng, L. W. T.; Zhu, X.; Howe, R. C. T.; Jones, C. G.; Hersam, M. C.; Hasan, T. Functional Inks and Printing of Two-Dimensional Materials. *Chem. Soc. Rev.* 2018, *47* (9), 3265–3300. https://doi.org/10.1039/C8CS00084K.
14. Paton, K. R.; Varrla, E.; Backes, C.; Smith, R. J.; Khan, U.; O'Neill, A.; Boland, C.; Lotya, M.; Istrate, O. M.; King, P.; Higgins, T.; Barwich, S.; May, P.; Puczkarski, P.; Ahmed, I.; Moebius, M.; Pettersson, H.; Long, E.; Coelho, J.; O'Brien, S. E.; McGuire, E. K.; Sanchez, B. M.; Duesberg, G. S.; McEvoy, N.; Pennycook, T. J.; Downing, C.; Crossley, A.; Nicolosi, V.; Coleman, J. N. Scalable Production of Large Quantities of Defect-Free Few-Layer Graphene by Shear Exfoliation in Liquids. *Nat. Mater.* 2014, *13*, 624. https://doi.org/10.1038/nmat3944https://www.nature.com/articles/nmat3944#supplementary-information.

15. Khan, U.; O'Neill, A.; Lotya, M.; De, S.; Coleman, J. N. High-Concentration Solvent Exfoliation of Graphene. *Small* 2010, *6*, 864–871. https://doi.org/10.1002/smll.200902066.
16. Zheng, M.; Lamberti, F.; Franco, L.; Collini, E.; Fortunati, I.; Bottaro, G.; Daniel, G.; Sorrentino, R.; Minotto, A.; Kukovecz, A.; Menna, E.; Silvestrini, S.; Durante, C.; Cacialli, F.; Meneghesso, G.; Maggini, M.; Gatti, T. A Film-Forming Graphene/Diketopyrrolopyrrole Covalent Hybrid with Far-Red Optical Features: Evidence of Photo-Stability. *Synth. Met.* 2019, *258*, 116201. https://doi.org/https://doi.org/10.1016/j.synthmet.2019.116201.
17. Ferrari, A. C.; Meyer, J. C.; Scardaci, V.; Casiraghi, C.; Lazzeri, M.; Mauri, F.; Piscanec, S.; Jiang, D.; Novoselov, K. S.; Roth, S.; Geim, A. K. Raman Spectrum of Graphene and Graphene Layers. *Phys. Rev. Lett.* 2006, *97*, 187401. https://doi.org/10.1103/PhysRevLett.97.187401.
18. Eckmann, A.; Felten, A.; Mishchenko, A.; Britnell, L.; Krupke, R.; Novoselov, K. S.; Casiraghi, C. Probing the Nature of Defects in Graphene by Raman Spectroscopy. *Nano Lett.* 2012, *12*, 3925–3930. https://doi.org/10.1021/nl300901a.
19. Malard, L. M.; Pimenta, M. A.; Dresselhaus, G.; Dresselhaus, M. S. Raman Spectroscopy in Graphene. *Phys. Rep.* 2009, *473*, 51–87. https://doi.org/https://doi.org/10.1016/j.physrep.2009.02.003.
20. Turner, P.; Hodnett, M.; Dorey, R.; Carey, J. D. Controlled Sonication as a Route to In-Situ Graphene Flake Size Control. *Sci. Rep.* 2019, *9*, 8710. https://doi.org/10.1038/s41598-019-45059-5.
21. Esmeryan, K. D.; Castano, C. E.; Bressler, A. H.; Abolghasemibizaki, M.; Fergusson, C. P.; Roberts, A.; Mohammadi, R. Kinetically Driven Graphite-like to Diamond-like Carbon Transformation in Low Temperature Laminar Diffusion Flames. *Diam. Relat. Mater.* 2017, *75*, 58–68. https://doi.org/https://doi.org/10.1016/j.diamond.2017.01.014.
22. Cunha, E.; Proença, M. F.; Costa, F.; Fernandes, A. J.; Ferro, M. A. C.; Lopes, P. E.; González-Debs, M.; Melle-Franco, M.; Deepak, F. L.; Paiva, M. C. Self-Assembled Functionalized Graphene Nanoribbons from Carbon Nanotubes. *ChemistryOpen* 2015, 4, 115–119. https://doi.org/10.1002/open.201402135
23. Barbera, V.; Brambilla, L.; Milani, A.; Palazzolo, A.; Castiglioni, C.; Vitale, A.; Bongiovanni, R.; Galimberti, M. Domino Reaction for the Sustainable Functionalization of Few-Layer Graphene. *Nanomaterials* 2019, *9*, 1-23. https://doi.org/10.3390/nano9010044.
24. Gatti, T.; Vicentini, N.; Mba, M.; Menna, E. Organic Functionalized Carbon Nanostructures for Functional Polymer-Based Nanocomposites. *Eur. J. Org. Chem.* 2016, *6*, 1071–1090. https://doi.org/doi:10.1002/ejoc.201501411.
25. Gabrielli, L.; Altoè, G.; Glaeske, M.; Juergensen, S.; Reich, S.; Setaro, A.; Menna, E.; Mancin, F.; Gatti, T. Controlling the Decoration of the Reduced Graphene Oxide Surface with Pyrene-Functionalized Gold Nanoparticles. *Phys. Status Solidi Basic Res.* 2017, *254*, 1700281 . https://doi.org/10.1002/pssb.201700281.
26. Barbera, V.; Brambilla, L.; Porta, A.; Bongiovanni, R.; Vitale, A.; Torrisi, G.; Galimberti, M. Selective Edge Functionalization of Graphene Layers with Oxygenated Groups by Means of Reimer–Tiemann and Domino Reimer–Tiemann/Cannizzaro Reactions. *J. Mater. Chem. A* 2018, *6*, 7749–7761. https://doi.org/10.1039/C8TA01606B.
27. Guerra, S.; Barbera, V.; Vitale, A.; Bongiovanni, R.; Serafini, A.; Conzatti, L.; Brambilla, L.; Galimberti, M. Edge Functionalized Graphene Layers for (Ultra) High Exfoliation in Carbon Papers and Aerogels in the Presence of Chitosan. *Materials* 2019, *13*, 39-56. https://doi.org/10.3390/ma13010039.